pH-Responsive Supramolecular Vesicles Based on Water-Soluble Pillar[6]arene and Ferrocene Derivative for Drug Delivery

Qunpeng Duan,[†] Yu Cao,[†] Yan Li,[‡] Xiaoyu Hu,[†] Tangxin Xiao,[†] Chen Lin,[†] Yi Pan,[†] and Leyong Wang*,[†]

[†]Key Laboratory of Mesoscopic Chemistry of MOE, Center for Multimolecular Chemistry, School of Chemistry and Chemical Engineering, Nanjing University, Nanjing 210093, China

[‡]State Key Laboratory of Bioelectronics and Jiangsu Key Laboratory of Biomaterials and Devices, School of Biological Science and Medical Engineering, Southeast University, Nanjing 210009, China

S *Supporting Information*

ABSTRACT: The drug delivery system based on supramolecular vesicles that were self-assembled by a novel host−guest inclusion complex between a water-soluble pillar[6]arene (**WP6**) and hydrophobic ferrocene derivative in water has been developed. The inclusion complexation between **WP6** and ferrocene derivative in water was studied by ^{1}H NMR, UV−vis, and fluorescence spectroscopy, which showed a high binding constant of $(1.27 \pm 0.42) \times 10^5 \, M^{-1}$ with 1:1 binding stoichiometry. This resulting inclusion complex could self-assemble into supramolecular

vesicles that displayed a significant pH-responsive behavior in aqueous solution, which were investigated by fluorescent probe technique, dynamic laser scattering, and transmission electron microscopy. Furthermore, the drug loading and *in vitro* drug release studies demonstrated that these supramolecular vesicles were able to encapsulate mitoxantrone (MTZ) to achieve MTZ-loaded vesicles, which particularly showed rapid MTZ release at low-pH environment. More importantly, the cellular uptake of these pH-responsive MTZ-loaded vesicles by cancer cells was observed by living cell imaging techniques, and their cytotoxicity assay indicated that unloaded vesicles had low toxicity to normal cells, which could dramatically reduce the toxicity of MTZ upon loading of MTZ. Meanwhile, MTZ-loaded vesicles exhibited comparable anticancer activity *in vitro* as free MTZ to cancer cells under examined conditions. This study suggests that such supramolecular vesicles have great potential as controlled drug delivery systems.
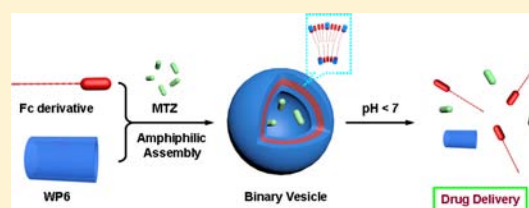
1. INTRODUCTION

Over the past three decades, the explosive growth of nanotechnology platforms has promoted the innovative revolution of the delivery of bioactive drug in pharmacology by developing new drug nanocarriers or drug delivery systems (DDS) that can dramatically enhance the bioavailability of drugs.[1] These drug nanocarriers or DDS are required to be "smart", which not only have to be constructed with well-defined structures to capture therapy drugs but also are able to release loaded therapy drugs in response to environmental stimuli, especially under some specific environment of some organs, intracellular space, or pathological sites.[2] Vesicles have been widely studied as one of nanocarriers or DDS since their discovery in the mid 1960s,[1c,3] due to their unique cavities that can efficiently encapsulate drugs. A wide variety of molecular building blocks were exploited for the construction of vesicles,[4] and among them supramolecular amphiphiles[5] with stimuli-responsive properties as building blocks to form vesicles are more promising in developing stimuli-responsive nanocarriers or DDS, since they can not only self-assemble into well-defined structures, such as vesicles, but also undergo conformational transitions in response to environmental stimuli. Up to now, several kinds of noncovalent interactions have been used to construct supramolecular amphiphiles, including hydrogen-bonding, charge-transfer, and $\pi \cdots \pi$ interactions, and so on.[6]

However, there are only a few reports on the formation of supramolecular vesicles from supramolecular amphiphiles based on host−guest interactions between macrocyclic hosts and guests.[7] Therefore, the construction of supramolecular vesicles from novel supramolecular amphiphiles through host−guest interactions, especially with stimuli-responsiveness, is of great interest and importance in application of biotechnology and biomedicine, particularly for drug delivery. Moreover, most of the main stimuli in DDS that are capable of triggering the release of loaded drugs are from the organism itself, such as the temperature, pH value, and the GSH concentration.[8] Considering the wide range of pH gradients presented in biological and physiological system,[9] the fabrication of pH-responsive supramolecular vesicles based on novel supramolecular amphiphiles for controlled drug encapsulation/release is of particular interest.

Pillararenes,[10] composed of hydroquinone units linked by methylene bridges at the *para*-positions, represent a particularly significant new class of macrocyclic hosts in supramolecular chemistry. Their intrinsic unique rigid and symmetrical pillar architecture and easy modification have endowed pillararenes with outstanding abilities to selectively bind various types of

guests. Consequently, pillararenes have received great attention in constructing various interesting supramolecular systems, including nanomaterials,[7k−m,11] chemosensors,[12] transmembrane channels,[13] and supramolecular polymers.[14] Most recently, we reported that the new guest, ferrocenium, can strongly bind per-butylated pillar[6]arene in organic solvents, but its reduced form, ferrocene, shows extremely weak binding affinity.[15] It is quite different from the reported binding behavior of ferrocene/ferrocenium with β-cyclodextrin in aqueous solution, where ferrocene can bind β-cyclodextrin more strongly than ferrocenium due to the hydrophobic effect in aqueous solution.[16] Therefore, we envisioned that ferrocene derivative might also strongly bind water-soluble pillar[6]arene (**WP6**) in water to achieve a stable inclusion complex due to the similar hydrophobic effect, which would be different from its binding behavior in organic solvents, and more importantly, if this resulting inclusion complex is amphiphilic, it would be possibly able to form supramolecular vesicles in water by self-assembly. Furthermore, **WP6** as the carboxylic sodium salt and its precipitation out of water as carboxylic acid could be reversibly adjusted by changing the solution pH,[71] which could allow the above proposed supramolecular vesicles to achieve pH responsiveness.

To the best of our knowledge, no example of pillararene-based supramolecular vesicels has been exploited for DDS. Therefore, we report herein a novel supramolecular amphiphilic inclusion complex between **WP6** and hydrophobic *N*-1-decyl-ferrocenylmethylamine (**G**) in aqueous solution, which was further applied to construct nanoscale supramolecular vesicles with pH responsiveness for drug delivery as schematically depicted in Scheme 1. Significantly, DDS constructed by such

Scheme 1. Schematic Illustration of the Formation of Supramolecular Vesicles and Their pH-Responsive Drug Release
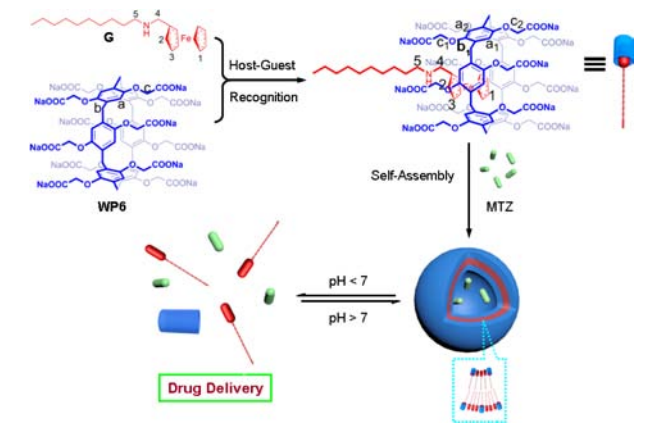
pillararene-based supramolecular vesicles for encapsulation and controlled release of anticancer drug mitoxantrone (MTZ) was realized for the first time. Meanwhile, the resulting MTZ-loaded supramolecular vesicles showed rapid MTZ release at low-pH environments, which is very important for the development of highly efficient DDS. More importantly, cellular uptake and cytotoxicity experiments of the MTZ-loaded supramolecular vesicles demonstrated the efficiency of such supramolecular vesicles for intracellular drug delivery and growth inhibition of cancer cells.

2. RESULTS AND DISCUSSION

Host−Guest Complexation Studies in Water. **WP6**[71] and **G**[17] were prepared according to the published procedures. The complexation between **WP6** and **G** in D_2O was first investigated by ^{1}H NMR spectroscopy. Since the guest molecule **G** is hydrophobic and exhibits poor solubility in water, the protons on **G** show weak absorption intensity in ^{1}H NMR spectrum. Figure 1 shows the ^{1}H NMR titration results
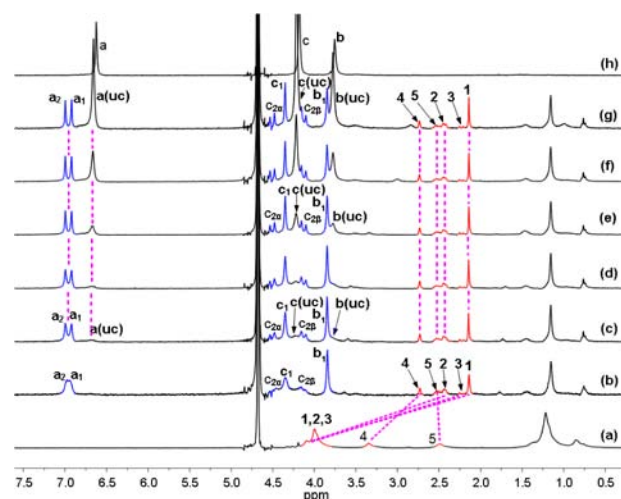
Figure 1. ^{1}H NMR spectra (D_2O, 298 K, 400 MHz) of **G** at a constant concentration of 0.72 mM with different concentrations (mM) of **WP6**: (a) 0.00, (b) 0.54, (c) 0.81, (d) 1.08, (e) 1.62, (f) 2.16, (g) 2.70, and (h) individual **WP6** (2.7 mM). The blue and red peaks correspond to complexed host and guest protons, respectively. Uncomplexed species are denoted by "uc".

of **WP6** with **G** in D_2O, from which the remarkable upfield chemical shifts of ferrocenyl proton resonances $H_{1−4}$ were observed upon addition of **WP6** due to the shielding effect of the electron-rich cavities of **WP6** for **G**, indicating the inclusion of the ferrocene moiety of **G** into the hydrophobic **WP6** cavity. The assignment of these ferrocenyl proton signals of the inclusion complex can be substantiated by the analysis of the [1]H−^{1}H COSY data (correlation spectroscopy; see Figure S1a). The spatial conformation of such inclusion complex can be further confirmed by 2D ROESY, which has a maximal observation limit at a spatial proximity of 5 Å.[18] From the 2D ROESY spectrum of a solution of **WP6** (2.16 mM) and **G** (0.72 mM) (Figure S2), intermolecular correlations were observed between protons H_1, H_2 on the ferrocene moiety and protons Ha_1, Ha_2 of **WP6**, respectively, confirming that the ferrocene moiety of **G** threaded into the cavity of **WP6**. Hence, all the above results suggested that a "tadpole-like" 1:1 inclusion complex (Figure S1b) between **WP6** and **G** was formed in aqueous solution, where the ferrocene moiety of **G** threaded into the cavity of **WP6** and the alkyl chain residue of **G** protruded out of the **WP6** cavity. In addition, the formation of a **WP6**⊃**G** inclusion complex is also supported by experimental observations on the enhanced solubility of **G** in aqueous media containing **WP6**. The conformation model of **WP6**⊃**G** inclusion complex in water was proposed as shown in Scheme 1.

The stoichiometry of complexation between **WP6** and **G** in water was further investigated by the continuous variation method (Job's plot method) using the UV−vis spectroscopy,

which confirmed the 1:1 binding stoichiometry between **WP6** and **G** (Figure S3). To determine their association constant in water, steady-state fluorescence spectra of **WP6** at varying **G** concentrations were recorded. As shown in Figure S4, upon addition of **G**, the fluorescence intensity of **WP6** (monitored at 330 nm) was gradually quenched, and the association constant of **WP6⊃G** was calculated to be $(1.27 \pm 0.42) \times 10^5$ M^{-1} by using a nonlinear curve-fitting method (Figure S5), which is much stronger than that of ferrocene with per-butylated pillar[6]arene (18 $\pm$ 0.5 M^{-1}) in organic solvents.[15] The highly strong formation of **WP6⊃G** inclusion complex in water might be mainly driven by hydrophobic interactions between the hydrophobic cavity of **WP6** and the hydrophobic ferrocene moiety of **G**.

Further evidence for the formation of the **WP6⊃G** inclusion complex was obtained by cyclic voltammetry experiments. As shown in Figure S6, in the aqueous solution of **G** with the presence of 1.0 equiv of **WP6**, the anodic peak current decreased compared with individual **G** solution, due to the inclusion of the ferrocene moiety of **G** into the cavity of **WP6**, which decreased the effective diffusion coefficient of the electroactive species.[19] In addition, upon addition of 1.0 equiv of **WP6** into **G** solution, the half-wave potential ($E_{1/2}$) associated with the one-electron oxidation of the ferrocene moiety of **G** decreased by ~58 mV, suggesting that the oxidized form of **G** (ferrocenium derivative) could form a more stable inclusion complex with **WP6** than the reduced form **G** in water.[19,20] For comparison, the association constant of **WP6** with ferrocenium (introduced as its tetrafluoroborate salt) in water was determined to be $(8.68 \pm 0.72) \times 10^7$ M^{-1} by fluorescent titration experiments with the 1:1 binding stoichiometry (Figures S8, S9), which is much stronger than that of **WP6** with **G** $((1.27 \pm 0.42) \times 10^5$ M$^{-1})$ in water and that of carbazole-functionalized pillar[6]arene with ferrocenium $((2.00 \pm 0.10) \times 10^4$ M$^{-1})$[15] in organic solvents. This stronger binding affinity of **WP6** with ferrocenium in water is possibly caused by the strong charge-transfer effect between electron-deficient ferrocenium and electron-rich cavity of **WP6**, which was supported by their UV−vis absorption spectroscopy (Figure S10). Furthermore, the formation of the inclusion complex between **WP6** and ferrocenium could also be supported by utilizing ^{1}H NMR spectroscopy to investigate the complexation between **WP6** and cobaltocenium (**Cob$^+$**, introduced as its hexafluorophosphate salt), an analogue of ferrocenium (Figure S11), due to the paramagnetic nature of ferrocenium which hinders the observation of its proton NMR resonances.

Construction of Supramolecular Binary Vesicles in Water Based on the Host−Guest Complexation of WP6 with G. After establishing the novel **WP6⊃G** supramolecular inclusion complex as a recognition motif in aqueous solution, we further utilized it to construct supramolecular vesicles, since such **WP6⊃G** inclusion complex has amphiphilic property where the **WP6** residue at one end shows hydrophilic and the alkyl chain residue of **G** at the other end shows hydrophobic. In order to investigate the amphiphilie assembly of such supramolecular inclusion complex, steady-state fluorescence measurement using pyrene as the probe was employed. The fluorescence intensities of various vibronic fine structures of the pyrene monomer show a strong dependence on the solvent environment, and the intensity of the 0−0 vibronic band (I_{373}) diminishes with the decrease of the solvent polarity.[21] Thus, the intensity of the first vibronic peak, i.e., I_{373}, can be taken as a

measure for the polarity of the environment. In the presence of micelles and other macromolecular systems, pyrene is preferentially solubilized in the interior hydrophobic regions (Stern region) of these aggregates,[22] resulting in a loss of fluorescence intensity. The fluorescence spectra of the solution of **WP6** with the increasing **G** concentration in the presence of pyrene probe molecules were shown in Figure S12, which displayed that the relative fluorescence intensity of pyrene dramatically decreased with the increasing **G** concentration. This obvious fluorescence quenching can be explained by the fact that nonpolar pyrene is solubilized near the Stern region in aggregates, which proves the formation of the amphiphilic aggregation with the fact that neither **WP6** nor **G** has tendency to self-aggregate in aqueous solution.[7m,23] Control experiments showed that the addition of **WP6** into the pyrene and **G** solution caused a large fluorescence quenching, but the replacement of **WP6** by its building subunit hydroquinone-O,O'-diacetic acid disodium salt (**M**) could not quench the fluorescence of the pyrene and **G** solution at all, which suggests that the addition of **M** into the **G** solution could not induce the formation of aggregation but **WP6** could (Figure 2), indicating that the host−guest complexation between **WP6** and **G** is undoubtedly the crucial factor leading to an amphiphilic assembly.
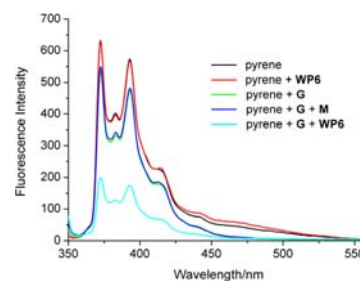

Figure 2. Fluorescence emission spectra of pyrene in aqueous solutions of **WP6**, **G**, **G + M**, and **G + WP6** at 25 °C. [**WP6**] = 0.00800 mM, [**G**] = 0.160 mM, [**M**] = 0.0400 mM, and [pyrene] = 1.00 μM.

Based on the above fluorescence experiments, we knew that **WP6⊃G** could form microaggregates based on the host−guest interactions between **WP6** and **G**. Therefore, it is necessary to determine the best molar ratio between **WP6** and **G** for constructing supramolecular aggregates by pyrene-based fluorescent probe technique. The fluorescence emission spectra of pyrene and its plot of fluorescent intensity at 373 nm as a function of the concentration of **WP6** added to the fixed 0.08 mM **G** solution were shown in Figure S13. Upon gradual addition of **WP6**, the fluorescent intensity of pyrene at 373 nm first decreased rapidly until the minimum was reached at a **WP6/G** ratio of 0.05 and then gradually increased thereafter upon further addition of **WP6**. This initially rapid decrease of the fluorescent intensity of pyrene indicated the formation of a higher-order complex between **WP6** and **G** with a tendency toward a supramolecular amphiphilic assembly, which was then disassembled upon further addition of **WP6** to gradually afford a simple 1:1 inclusion complex. The inflection was observed at the **WP6/G** molar ratio of 0.05, which means that, in the present **WP6-G** system, the best molar ratio for the amphiphilic assembly is 1:20 (**WP6:G**). Based on this best molar ratio, the critical aggregation concentration (CAC) of **G** with **WP6** was

determined to be $(1.27 \pm 0.01) \times 10^{-4}$ M using concentration-dependent conductivity (Figure S14).

The solution of **WP6** and **G** in the best molar ratio for amphiphilic assembly in water exhibits a clear Tyndall effect (Figure 3a), indicating the existence of abundant nanoparticles.
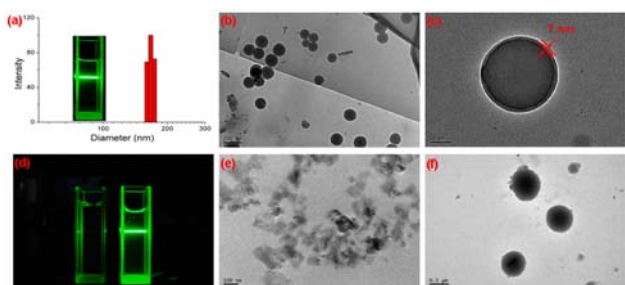

Figure 3. (a) DLS data of the **WP6** + **G** aggregates. Inset: Photo showing the Tyndall effect of **WP6** + **G** aggregates. TEM images: (b) **WP6** + **G** aggregates; (c) enlarged image of b. (d) Tyndall effect of **WP6** + **G** aggregates after the solution pH was adjusted to 6.0 (left) and after the solution pH was adjusted to 7.4 (right). TEM images: (e) **WP6** + **G** aggregates after the solution pH was adjusted to 6.0; (f) **WP6** + **G** aggregates after the solution pH was adjusted to 7.4. [**WP6**] = 0.0080 mM, and [**G**] = 0.16 mM.

Furthermore, in order to indentify the self-assembly size and morphology of this **WP6⊃G** supramolecular amphiphile, dynamic laser scattering (DLS) and transmission electron microscopy (TEM) were carried out. The DLS result showed that the **WP6⊃G** supramolecular amphiphile formed spectacular aggregates with a narrow size distribution, giving an average diameter of 167 nm (Figure 3a), and TEM images showed the hollow spherical morphology with an average diameter ~130 nm, convincingly indicating the formation of vesicular structure (Figure 3b). The fact that the diameter of vesicles measured by DLS is slightly larger than that found by TEM is reasonable, because TEM and DLS showed solid and swollen vesicles, respectively.[7c] What is more, the thickness of the hollow vesicles was calculated to be ~7 nm from their TEM image (Figure 3c). Considering that the extended length of two molecules of inclusion complexes calculated by Chem3D is around 5.2 nm, the vesicles may possess a bilayer structure with two hydrophilic carboxylate shell layers and one hydrophobic alkyl chain core layer, as shown in Scheme 1. Furthermore, in order to examine the stability of these vesicles, ζ-potential was measured,[24] which was negative (-26.30 ± 5.38 mV) as shown in Figure S15, meaning that the repulsive forces among vesicles exist, and the stability of vesicles can be manifested.

pH Responsiveness of the Supramolecular Binary Vesicles. Stimuli-responsive supramolecular amphiphiles that can self-assemble into nanoaggregates capable of responding to changes in environmental conditions are of extreme interest for smart drug delivery applications.[25] **WP6** has been demonstrated to show pH responsiveness in aqueous solution,[71] therefore, we envisioned that the present vesicles formed from the supramolecular amphiphile **WP6⊃G** are expected to show pH sensitivity.[26] As expected, the Tyndall effect for the above **WP6** + **G** solution disappeared (Figure 3d) after adjusting the solution pH to 6.0 accompanied by a dramatic decrease of scattering intensity measured by DLS, and meanwhile, no vesicle could be found in the TEM image any more (Figure 3e). All these results indicated the disassembly of the above supramolecular vesicles by adjusting the solution pH to 6.0.

However, when the pH was adjusted back to pH slightly higher than 7.0, vesicles were reformed in solution as shown in Figure 3f, which was also confirmed by DLS experiment (Figure S16), proving the pH-responsive assembly and disassembly of the supramolecular amphiphile **WP6⊃G**.

MTZ Encapsulation and *in Vitro* Release. MTZ is widely used to treat a broad range of solid malignant tumors, which works by interfering with DNA synthesis through intercalation and stabilization of DNA topoisomerase II cleavable complex.[27] Herein, MTZ was used as a model drug to evaluate the encapsulation efficiency of the above resulting supramolecular vesicles and their release behavior of loaded drug. To prepare MTZ-loaded vesicles, an aqueous solution of MTZ was quickly added into a freshly prepared aqueous solution of **WP6** and **G** (**WP6**:**G** = 1:20, molar ratio), and after standing overnight, unloaded MTZ molecules were removed by dialysis against water. As a result, MTZ was successfully loaded into the supramolecular vesicles formed between **WP6** and **G**. Compared with the MTZ-unloaded vesicular solution, the absorption of MTZ-loaded vesicular solution from 610 to 660 nm becomes much stronger (Figure 4), which represents the
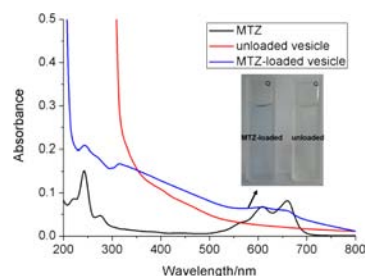
Figure 4. UV−vis absorption spectra of the solution of MTZ, unloaded vesicles, and MTZ-loaded vesicles at 25 °C in water. Inset: color change of MTZ-loaded vesicles (left) compared with unloaded vesicles (right).

characteristic absorption of MTZ in aqueous solution. Meanwhile, the MTZ-loaded vesicular solution turns to light blue compared with the colorless MTZ-unloaded vesicular solution after removing unloaded MTZ molecules by dialysis, demonstrating that MTZ was successfully encapsulated into the vesicles (Figure 4). More intuitively, the MTZ-loaded vesicles showed a darker interior in TEM observations (Figure 5a,b), confirming that MTZ molecules were loaded into the
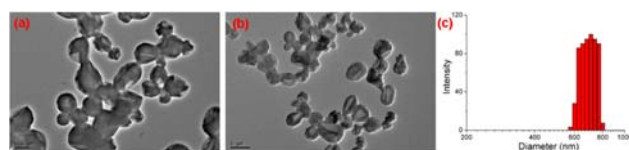
Figure 5. (a,b) TEM images of MTZ-loaded vesicles. (c) DLS data of MTZ-loaded vesicles.

vesicular interior under the condition of sample preparation. DLS results showed that these MTZ-loaded vesicles are much larger in size (average diameter of 694 nm, Figure 5c) than those of the unloaded (average diameter of 167 nm), which is consistent with the size increase of vesicles after the encapsulation of guests reported before.[28] According to UV−vis absorption spectra, the MTZ encapsulation efficiency was calculated to be 11.2%, indicating a good drug-loading capability of the above supramolecular vesicles.

The release behavior of MTZ from the MTZ-loaded vesicles could be controlled by changing solution pH. The release profiles of MTZ under the physiological condition (pH 7.4) and acidic conditions (pH 6.5 and 4.0) are presented in Figure 6. The cumulative release of MTZ was only ~13% within 24 h
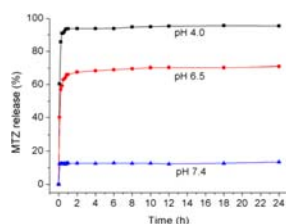

Figure 6. pH-Responsive MTZ release profiles of the MTZ-loaded vesicles in the release media of different pH values.

under the physiological conditions. However, by adjusting the solution pH to acidity MTZ was released in significant amounts from the MTZ-loaded vesicles into the external environment, i.e., 71% at pH 6.5 and 95% release efficiency at pH 4.0 within 24 h. In particular, from the profiles, rapid release could be observed in acidic condition in the first five minutes. Since the microenvironment of tumor cells is acidic for both intracellular and extracellular compartments, the rapid release of MTZ from MTZ-loaded vesicles can be triggered by the acidic micro-environment of tumor cells,[29] which is extremely significant for specific targeted therapy. This pH-responsive rapid drug release phenomenon can be well explained by considering a pH-triggered vesicles collapse, which is concomitant with release of the encapsulated MTZ drug. As a consequence, this rapid release behavior which shows a good response to physiologically relevant pH (pH 4.0−7.4) makes MTZ-loaded vesicles ideal candidates for DDS.

Cellular Uptake and *in Vitro* Cytotoxicity. To further investigate the cellular uptake of the **WP6⊃G**-based pH-responsive drug delivery system, SMMC-7721 cancer cells were incubated with MTZ-loaded vesicles. The fluorescence confocal image demonstrated that in bright-field the presence of SMMC-7721 cancer cells was observed (Figure S17a), and red fluorescence from MTZ-loaded vesicles could be observed in the cell body (Figure S17b), indicating that MTZ-loaded vesicles have entered into the cancer cells.

Although the MTZ-loaded vesicles were internalized within the SMMC-7721 cancer cells, the potential cytotoxicity of unloaded vesicles and MTZ-loaded vesicles to normal cells and the anticancer activity of the MTZ-loaded vesicles to cancer cell need to be investigated using the methyl thiazole tetrazolium (MTT) cell-survival assay for their future potential clinical applications. We initially incubated unloaded vesicles, MTZ, and MTZ-loaded vesicles with NIH3T3 cells (normal cells), and the relative viabilities of NIH3T3 cells in different groups were recorded from days 1 to 4. As shown in Figure 7a, we found that the relative viability of NIH3T3 cells incubated with unloaded vesicles group was over 75% after 96 h, indicating low cytotoxicity of the unloaded vesicles, which suggested that the supramolecular vesicles based on **WP6⊃G** employed in this work are promising drug carriers. Furthermore, it is quite interesting and meaningful that the viabilities of living cells in the MTZ-loaded vesicle group are always much higher than those in the MTZ group from days 2 to 4 ($P < 0.05$), and the morphology of living cells in the MTZ-loaded vesicle group is better than that in the MTZ group even after 96 h (Figure
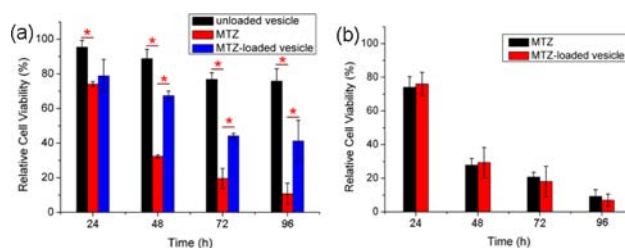
Figure 7. (a) Effect of unloaded vesicles, MTZ, and MTZ-loaded vesicles on viability of NIH3T3 cells at different times. (b) Anticancer activity of free MTZ and MTZ-loaded vesicles in SMMC-7721 cells at different times. Statistically significant differences were observed ($p < 0.05$) (*).

8b,c), both of which imply that the systemic toxicity of MTZ was remarkably reduced upon its loading by the supramolecular
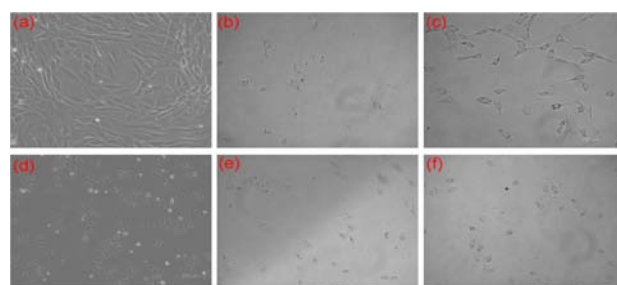
Figure 8. Images of living NIH3T3 cells in (a) blank, (b) MTZ, and (c) MTZ-loaded vesicle groups after 96 h. Images of living SMMC-7721 cells in (d) blank, (e) MTZ, and (f) MTZ-loaded vesicle groups after 96 h.

vesicles. MTZ and MTZ-loaded vesicles were then incubated with SMMC-7721 cells (cancer cells), respectively, and the relative viabilities of SMMC-7721 cells in each group were recorded from days 1 to 4. As shown in Figure 7b, the cytotoxicity assay showed that MTZ-loaded vesicles have a similar relative cell viability to the cancer cells compared with free MTZ under examined conditions, which also can be supported by cell images after 96 h (Figure 8e,f) for the MTZ and MTZ-loaded vesicle groups, respectively. All the above results imply that loading of MTZ by supramolecular vesicles does not affect the therapeutic effects of MTZ for cancer cells. Therefore, the cytotoxicity of MTZ-loaded vesicles could be obviously reduced to normal cells, due to their stability in the physiological environment (pH = 7.4), whereas compared with normal cells, cancer cells were able to disassemble the MTZ-loaded vesicles accompanying with the release of MTZ, due to its weakly acidic intracellular environment.[30] As a consequence, the pH-sensitive feature of the supramolecular vesicles based on **WP6⊃G** impels the release of loaded drug MTZ from vesicles in the cancer cells.

3. CONCLUSIONS

In conclusion, we have successfully constructed novel supra-molecular vesicles self-assembled by the new host−guest amphiphilic inclusion complex between **WP6** and **G** in water, which display a significant pH-responsive behavior. Further-more, their MTZ drug loading and *in vitro* drug release experiments demonstrated that MTZ was successfully encapsu-lated into the vesicles, and particularly, the resulting MTZ-loaded vesicles exhibit an excellent pH responsiveness and

quick release of MTZ at acidic pH environment, enabling them to be suitable for application in controlled drug release. Finally, the cytotoxicity assay of normal cells indicated that unloaded vesicles had low toxicity and loading of MTZ by vesicles could dramatically reduce the toxicity of MTZ to normal cells. Meanwhile, the cytotoxicity assay of cancer cells confirmed that the MTZ-loaded vesicles could be successfully uptaken by cancer cells, and the loading of MTZ by supramolecular vesicles does not affect the therapeutic effects of MTZ for cancer cells. These present novel supramolecular vesicles constructed by **WP6** and **G** in water are expected to have great potential applications in controlled release and drug delivery.

4. EXPERIMENTAL SECTION

Materials Preparation. Pyrene (98%) was purchased from J&K Chemical Company. Mitoxantrone (MTZ) (>98%) was provided by Melone Pharmaceutical Co., Ltd. (Dalian, China). Both of them were used without further purification. **WP6** and *N*-1-decyl-ferrocenylmethylamine were synthesized and purified according to previously reported procedures,[7l,17] and they were identified by ^{1}H NMR spectroscopy in D_2O, performed on a Bruker Advance DMX 300 MHz spectrometer, mass spectrometry, performed on Finnigan Mat TSQ 7000 instruments. The CAC determination of **WP6⊃G** was carried out on a DDS-307A instrument according to procedures reported by Huang's group.[7m]

ζ-Potential Measurement. ζ-potential measurement was performed at 25 °C on a Zeta sizer-Nano Z (Malvern Instruments Ltd., Worcestershire, U.K.) using the Smoluchowski model for the calculation of the ζ-potential from the measured electrophoretic mobility.

MTZ Loading and Release of WP6⊃G Vesicles. MTZ-loaded vesicles were prepared as follows: A certain amount of MTZ was added to a solution containing **WP6** and **G** (1% THF was added to improve the solubility of **G**), and then water was added until the volume of the solution reached 50 mL. The ultimate concentrations of MTZ, **G**, and **WP6** were 0.168, 0.16, and 0.008 mM, respectively. After standing overnight, the prepared MTZ-loaded vesicles were purified by dialysis (molecular weight cutoff 15 000) in distilled water for several times until the water outside the dialysis tube exhibited negligible MTZ fluorescence.

The MTZ encapsulation efficiency was calculated by the following equation:[7g]

$$\text{encapsulation efficiency}(\%) = (m_{\text{MTZ-loaded}}/m_{\text{MTZ}}) \times 100$$

where $m_{\text{MTZ-loaded}}$ and m_{MTZ} are mass of MTZ encapsulated in vesicles and mass of MTZ added, respectively. The mass of MTZ was measured by a UV spectrophotometer at 660 nm and calculated as relative to a standard calibration curve in the concentrations from 0.37 to 6.3 μg/mL in water.

0.05 M tris-HCl (pH = 7.4), 0.2 M sodium acetate (pH = 4.0), and 0.1 M citrate (pH = 6.5) buffer solutions were used as drug release media to simulate normal physiological conditions and the intracellular conditions of tumor. In a typical release experiment, 1.6 mL of MTZ-loaded vesicles were added into 8.4 mL of appropriate release medium at 37 °C. At selected time intervals, 3 mL of the release media was taken out for measuring the released MTZ concentrations by the UV–vis absorption technique and then was returned to the original release media. The concentration of MTZ was determined by measurement of absorbance at 660 nm using a standard absorbance vs concentration curve constructed for MTZ in the corresponding release buffer. By presenting the vesicles to very low pH (the solution of HCl, pH = 2), a nearly 100% release of MTZ from MTZ-loaded vesicles could be obtained.

UV–vis Absorption and Fluorescence Emission Spectra. UV–vis spectra were recorded in a quartz cell (light path 10 mm) on a Perkin-Elmer Lambda 35 UV–vis Spectrometer. Steady-state fluorescence spectra were recorded in a conventional quartz cell (light path 10 mm) on a Perkin-Elmer LS55 Fluorescence Spectrometer.

TEM and DLS Experiments. TEM images were recorded on a JEM-2100 instrument. The sample for TEM measurements was prepared by dropping the solution onto a carbon-coated copper grid. DLS measurements were performed under a Brookhaven BI-9000AT system (Brookhaven Instruments Corporation, U.S.A.) equipped with a 200 mW laser light and operating at λ = 532 nm.

Electrochemical Experiments. The cyclic voltammetric measurements were performed in a three-electrode cell using a CHI812B electrochemical workstation at room temperature. All the samples were prepared in aqueous solution and deoxygenated by purging with dry nitrogen before each experiment. The glassy carbon working electrode was polished with 0.05 μm BAS alumina suspension on a brown Texmet polishing pad, sonicated in distilled water for a few minutes to remove any residual alumina particles, and then washed with ethanol and distilled water before use. A platinum plate (Pt) was used as the counter electrode with a saturated calomel electrode (SCE) as the reference electrode. Both of the concentrations of **WP6** and **G** were 1.00×10^{-4} M.

In Vitro **Cell Assay.** Cellular uptake of the MTZ-loaded vesicles in live cells was investigated by fluorescence microscope (IX-81, Olympus) in SMMC-7721 cell line. SMMC-7721 cells (5×10^4 cells/dish) were seeded in glass-bottomed culture dish with 5 mL DMEM medium containing 10% fetal bovine serum, supplemented with 50 U/mL^{-1} penicillin and 50 U/mL^{-1} streptomycin at 37 °C in the CO_2 incubator. After incubation for 24 h, the cells were treated with 0.315 μg/mL MTZ-loaded vesicles for the study on nonspecific endocytosis of the MTZ-loaded vesicles. Fluorescence images of the cells were obtained with the microscope at 37 °C in a live cell chamber (INUS-WSKM-F1, Olympus) using a 10/0.4 NA objective. The fluorescence images were processed using cellSens software (Olympus).

The relative cytotoxicities of the vesicles, MTZ, and MTZ-loaded vesicles against NIH3T3 cells and SMMC-7721 cells were evaluated *in vitro* by MTT assay, respectively. Briefly, the cells were seeded in 96-well plates at a density of 10^4 cells per well in 200 μL complete DMEM containing 10% fetal bovine serum, supplemented with 50 U/mL^{-1} penicillin and 50 U/mL^{-1} streptomycin, and cultured in 5% CO_2 at 37 °C for 24 h. Then NIH3T3 cells were incubated with unloaded vesicle, MTZ, and MTZ-loaded vesicle, respectively. SMMC-7721 cells were subsequently incubated with MTZ and MTZ-loaded vesicle, respectively. The ultimate concentrations of MTZ, **WP6**, and **G** were 0.47, 0.27, and 5.33 μM, respectively. At the end of each incubation (24, 48, 72, or 96 h), the cells were washed and replenished with fresh culture medium, which were further incubated for 2 h. Subsequently, 20 μL of MTT solution was added into each cell and incubated for another 4 h. After that, the medium containing MTT was removed and dimethyl sulfoxide (100 μL) was added to each well to dissolve the MTT formazan crystals. Finally, the plates were shaken for 10 min, and the absorbance of formazan product was measured at 490 nm by a microplate reader (BioTek ELx808). Untreated cells in media were used as the blank control. All experiments were carried out with three replicates. The cytotoxicity was expressed as the percentage of the cell viability as compared with the blank control.

Statistical Analysis. Differences between treatment groups were statistically analyzed using the paired Student's *t*-test. A statistically significant difference was reported if $p < 0.05$ or less. The data were expressed as mean ± standard deviation from at least three separate experiments.

■ ASSOCIATED CONTENT

Ⓢ Supporting Information

Experimental procedures and supporting figures. This material is available free of charge via the Internet http://pubs.acs.org.

■ AUTHOR INFORMATION

Corresponding Author

lywang@nju.edu.cn

Notes

The authors declare no competing financial interest.

REFERENCES

(1) (a) LaVan, D. A.; McGuire, T.; Langer, R. *Nat. Biotechnol.* **2003**, *21*, 1184−1191. (b) Duncan, R. *Nat. Rev. Drug Discovery* **2003**, *2*, 347−360. (c) Allen, T. M.; Cullis, P. R. *Science* **2004**, *303*, 1818−1822. (d) MaHam, A.; Tang, Z.; Wu, H.; Wang, J.; Lin, Y. *Small* **2009**, *5*, 1706−1721. (e) Peer, D.; Karp, J. M.; Hong, S.; Farokhzad, O. C.; Margalit, R.; Langer, R. *Nat. Nanotechnol.* **2007**, *2*, 751−760. (f) Ma, N.; Li, Y.; Xu, H.; Wang, Z.; Zhang, X. *J. Am. Chem. Soc.* **2010**, *132*, 442−443. (g) Devadasu, V. R.; Bhardwaj, V.; Kumar, M. N. V. R. *Chem. Rev.* **2013**, *113*, 1686−1735.

(2) (a) Danhier, F.; Feron, O.; Préat, V. *J. Controlled Release* **2010**, *148*, 135−146. (b) Peppas, N. A.; Wood, K. M.; Blanchette, J. O. *Expert Opin. Biol. Ther.* **2004**, *4*, 881−887.

(3) (a) Bangham, A. D.; Standish, M. M.; Watkins, J. C. *J. Mol. Bio.* **1965**, *13*, 238−252. (b) Shen, Y.; Jin, E.; Zhang, B.; Murphy, C. J.; Sui, M.; Zhao, J.; Wang, J.; Tang, J.; Fan, M.; Krik, V. E.; Murdoch, W. J. *J. Am. Chem. Soc.* **2010**, *132*, 4259−4265. (c) Soussan, E.; Cassel, S.; Blanzat, M.; Rico-Lattes, I. *Angew. Chem., Int. Ed.* **2009**, *48*, 274−288. (d) Zhang, Z.; Cao, W.; Jin, H.; Lovell, J. F.; Yang, M.; Ding, L.; Chen, J.; Corbin, I.; Luo, Q.; Zheng, G. *Angew. Chem., Int. Ed.* **2009**, *48*, 9171−9175. (e) Sivakumar, S.; Bansal, V.; Cortez, C.; Chong, S. F.; Zelikin, A. N.; Caruso, F. *Adv. Mater.* **2009**, *21*, 1820−1824.

(4) Ravoo, B. J. In *Supramolecular Chemistry: from Molecules to Nanomaterials*; Steed, J. W., Gale, P. A., Eds.; John Wiley & Sons Ltd.: Chichester, U.K., 2012; Vol. 2, pp 501−514.

(5) (a) Zhang, X.; Wang, C. *Chem. Soc. Rev.* **2011**, *40*, 94−101. (b) Wang, C.; Wang, Z.; Zhang, X. *Acc. Chem. Res.* **2012**, *45*, 608−618.

(6) (a) Kimizuka, N.; Kawasaki, T.; Kunitake, T. *J. Am. Chem. Soc.* **1993**, *115*, 4387−4388. (b) Kimizuka, N.; Kawasaki, T.; Hirata, K.; Kunitake, T. *J. Am. Chem. Soc.* **1998**, *120*, 4094−4104. (c) Zhang, X.; Chen, Z.; Würthner, F. *J. Am. Chem. Soc.* **2007**, *129*, 4886−4887. (d) Kim, K.; Jeon, W. S.; Kang, J.-K.; Lee, J. K.; Jon, S. Y.; Kim, T.; Kim, K. *Angew. Chem., Int. Ed.* **2003**, *42*, 2293−2296. (e) Pisula, W.; Kastler, M.; Wasserfallen, D.; Robertson, J. W. F.; Nolde, F.; Kohl, C.; Müllen, K. *Angew. Chem., Int. Ed.* **2006**, *45*, 819−823. (f) Wang, Y.; Ma, N.; Wang, Z.; Zhang, X. *Angew. Chem., Int. Ed.* **2007**, *46*, 2823−2826. (g) Wang, C.; Yin, S.; Chen, S.; Xu, H.; Wang, Z.; Zhang, X. *Angew. Chem., Int. Ed.* **2008**, *47*, 9049−9052. (h) Ko, Y. H.; Kim, E.; Hwang, I.; Kim, K. *Chem. Commun.* **2007**, 1305−1315. (i) Bize, C.; Garrigues, J.-C.; Blanzat, M.; Rico-Lattes, I.; Bistri, O.; Colasson, B.; Reinaud, O. *Chem. Commun.* **2010**, *46*, 586−588.

(7) (a) Jeon, Y. J.; Bharadwaj, P. K.; Choi, S. W.; Lee, J. W.; Kim, K. *Angew. Chem., Int. Ed.* **2002**, *41*, 4474−4476. (b) Jing, B.; Chen, X.; Wang, X.; Yang, C.; Xie, Y.; Qiu, H. *Chem.−Eur. J.* **2007**, *13*, 9137−9142. (c) Zou, J.; Tao, F.; Jiang, M. *Langmuir* **2007**, *23*, 12791−12794. (d) Zhou, Q.; Wang, H.; Gao, T.; Yu, Y.; Ling, B.; Mao, L.; Zhang, H.; Meng, X.; Zhou, X. *Chem. Commun.* **2011**, *47*, 11315−11317. (e) Yan, Q.; Yuan, J.; Cai, Z.; Xin, Y.; Kang, Y.; Yin, Y. *J. Am. Chem. Soc.* **2010**, *132*, 9268−9270. (f) Wang, K.; Guo, D.; Liu, Y. *Chem.−Eur. J.* **2010**, *16*, 8006−8011. (g) Wang, K.; Guo, D.; Wang, X.; Liu, Y. *ACS Nano* **2011**, *5*, 2880−2894. (h) Guo, D.; Wang, K.; Wang, Y.; Liu, Y. *J. Am. Chem. Soc.* **2012**, *134*, 10244−10250. (i) Tao, W.; Liu, Y.; Jiang, B.; Yu, S.; Huang, W.; Zhou, Y.; Yan, D. *J. Am. Chem. Soc.* **2012**, *134*, 762−764. (j) Jiao, D.; Geng, J.; Loh, X. J.; Das, D.; Lee, T.-C.; Scherman, O. A. *Angew. Chem., Int. Ed.* **2012**, *51*, 9633−9637. (k) Yu, G.; Han, C.; Zhang, Z.; Chen, J.; Yan, X.; Zheng, B.; Liu, S.; Huang, F. *J. Am. Chem. Soc.* **2012**, *134*, 8711−8717. (l) Yu, G.; Xue, M.; Zhang, Z.; Li, J.; Han, C.; Huang, F. *J. Am. Chem. Soc.* **2012**, *134*, 13248−

13251. (m) Yu, G.; Zhou, X.; Zhang, Z.; Han, C.; Mao, Z.; Gao, C.; Huang, F. *J. Am. Chem. Soc.* **2012**, *134*, 19489−19497.

(8) (a) Ghadiali, J. E.; Stevens, M. M. *Adv. Mater.* **2008**, *20*, 4359−4363. (b) Gil, E. S.; Hudson, S. M. *Prog. Polym. Sci.* **2004**, *29*, 1173−1222. (c) Wei, H.; Cheng, S. X.; Zhang, X. Z.; Zhuo, R. X. *Prog. Polym. Sci.* **2009**, *34*, 893−910. (d) Saito, G.; Swansonb, J. A.; Lee, K. D. *Adv. Drug Delivery Rev.* **2003**, *55*, 199−215.

(9) Du, J.; O'Reilly, R. K. *Soft Matter* **2009**, *5*, 3544−3561.

(10) (a) Ogoshi, T.; Kanai, S.; Fujinami, S.; Yamagishi, T. A.; Nakamoto, Y. *J. Am. Chem. Soc.* **2008**, *130*, 5022−5023. (b) Xue, M.; Yang, Y.; Chi, X.; Zhang, Z.; Huang, F. *Acc. Chem. Res.* **2012**, *45*, 1294−1308. (c) Cragg, P. J.; Sharma, K. *Chem. Soc. Rev.* **2012**, *41*, 597−607. (d) Ogoshi, T. *J. Incl. Phenom. Macrocycl. Chem.* **2012**, *72*, 247−262.

(11) (a) Yao, Y.; Xue, M.; Chen, J.; Zhang, M.; Huang, F. *J. Am. Chem. Soc.* **2012**, *134*, 15712−15715. (b) Zhang, H.; Ma, X.; Guo, J.; Nguyen, K. T.; Zhang, Q.; Wang, X.-J.; Yan, H.; Zhu, L.; Zhao, Y. *RSC Adv.* **2013**, *3*, 368−371. (c) Nishimura, T.; Sanada, Y.; Matsuo, T.; Okobira, T.; Mylonas, E.; Yagi, N.; Sakurai, K. *Chem. Commun.* **2013**, *49*, 3052−3054. (d) Li, H.; Chen, D.-X.; Sun, Y.-L.; Zheng, Y.; Tan, L.-L.; Weiss, P.; Yang, Y.-W. *J. Am. Chem. Soc.* **2013**, *135*, 1570−1576. (e) Sun, Y.-L.; Yang, Y.-W.; Chen, D.-X.; Wang, G.; Zhou, Y.; Wang, C.-Y.; Stoddart, J. F. *Small* **2013**, DOI: 10.1002/smll.201300445.

(12) (a) Yu, G.; Zhang, Z.; Han, C.; Xue, M.; Zhou, Q.; Huang, F. *Chem. Commun.* **2012**, *48*, 2958−2960. (b) Sun, S.; Hu, X.-Y.; Chen, D.; Shi, J.; Dong, Y.; Lin, C.; Pan, Y.; Wang, L. *Polym. Chem.* **2013**, *4*, 2224−2229. (c) Shu, X.; Chen, S.; Li, J.; Chen, Z.; Weng, L.; Jia, X.; Li, C. *Chem. Commun.* **2012**, *48*, 2967−2969. (d) Li, C.; Han, K.; Li, J.; Zhang, H.; Ma, J.; Shu, X.; Chen, Z.; Weng, L.; Jia, X. *Org. Lett.* **2011**, *14*, 42−45.

(13) (a) Hu, X.-B.; Chen, Z.; Tang, G.; Hou, J.-L.; Li, Z.-T. *J. Am. Chem. Soc.* **2012**, *134*, 8384−8387. (b) Si, W.; Chen, L.; H, X.-B.; Tang, G.; Chen, Z.; Hou, J.-L.; Li, Z.-T. *Angew. Chem., Int. Ed.* **2011**, *50*, 12564−12568. (c) Chen, L.; Si, W.; Zhang, L.; Tang, G.; Li, Z.-T.; Hou, J.-L. *J. Am. Chem. Soc.* **2013**, *135*, 2152−2155.

(14) (a) Zhang, Z.; Luo, Y.; Chen, J.; Dong, S.; Yu, Y.; Ma, Z.; Huang, F. *Angew. Chem., Int. Ed.* **2011**, *50*, 1397−1401. (b) Guan, Y.; Ni, M.; Hu, X.; Xiao, T.; Xiong, S.; Lin, C.; Wang, L. *Chem. Commun.* **2012**, *48*, 8529−8531. (c) Hu, X.-Y.; Zhang, P.; Wu, X.; Xia, W.; Xiao, T.; Jiang, J.; Lin, C.; Wang, L. *Polym. Chem.* **2012**, *3*, 3060−3063. (d) Hu, X.-Y.; Wu, X.; Duan, Q.; Xiao, T.; Li, C.; Wang, L. *Org. Lett.* **2012**, *14*, 4826−4829.

(15) Xia, W.; Hu, X.; Chen, Y.; Liu, Y.; Lin, C.; Wang, L. *Chem. Commun.* **2013**, *49*, 5085−5087.

(16) Isnin, R.; Salam, C.; Kaifer, A. E. *J. Org. Chem.* **1991**, *56*, 35−41.

(17) Baramee, A.; Coppin, A.; Mortuaire, M.; Pelinski, L.; Tomavo, S.; Brocard, J. *Bioorg. Med. Chem.* **2006**, *14*, 1294−1302.

(18) Schneider, H.-J.; Hacket, F.; Rüdiger, V.; Ikeda, H. *Chem. Rev.* **1998**, *98*, 1755−1786.

(19) (a) Matsue, T.; Evans, D. H.; Osa, T.; Kobayashi, N. *J. Am. Chem. Soc.* **1985**, *107*, 3411−3417. (b) Kaifer, A. E. *Acc. Chem. Res.* **1999**, *32*, 62−71. (c) Hapiot, F.; Tilloy, S.; Monflier, E. *Chem. Rev.* **2006**, *106*, 767−781. (d) Harada, A. *Acc. Chem. Res.* **2001**, *34*, 456−464.

(20) Coluccini, C.; Sharma, A. K.; Merli, D.; Vander Griend, D.; Mannucci, B.; Pasini, D. *Dalton Trans.* **2011**, *40*, 11719−11725.

(21) Kalyanasundaram, K.; Thomas, J. K. *J. Am. Chem. Soc.* **1977**, *99*, 2039−2044.

(22) (a) Menger, F. M. *Acc. Chem. Res.* **1979**, *12*, 111−117. (b) Baudry, Y.; Bollot, G.; Gorteau, V.; Litvinchuk, S.; Mareda, J.; Nishihara, M.; Pasini, D.; Perret, F.; Ronan, D.; Sakai, N.; Shah, M. R.; Som, A.; Sordé, N.; Talukdar, P.; Tran, D.-H.; Matile, S. *Adv. Funct. Mat.* **2006**, *16*, 169−179.

(23) Zhang, H.; An, W.; Liu, Z.; Hao, A.; Hao, J.; Shen, J.; Zhao, X.; Sun, H.; Sun, L. *Carbohydr. Res.* **2010**, *345*, 87−96.

(24) Wiese, G. R.; Healy, T. W. *Trans. Faraday Soc.* **1970**, *66*, 490−499.

(25) (a) Ariga, K.; Ji, Q.; Hill, J. P.; Kawazoe, N.; Chen, G. *Expert Opin. Biol. Ther.* **2009**, *9*, 307−320. (b) Mccarley, R. L. *Annu. Rev. Anal. Chem.* **2012**, *5*, 391−411.

(26) Disassembly of supramolecular vesicles formed from **WP6** and **G** in acidic conditions could be mainly caused by the precipitate of pillar[6]arene carboxylic acid, and the protonation of the secondary amine group of the guest might be also responsible for the disassembly of the supramolecular vesicles.

(27) (a) Parker, B. S.; Buley, T.; Evison, B. J.; Cutts, S. M.; Neumann, G. M.; Iskander, M. N.; Phillips, D. R. *J. Biol. Chem.* **2004**, *279*, 18814−18823. (b) Mazerski, J.; Martelli, S.; Borowski, E. *Acta Biochim. Pol.* **1998**, *45*, 1−11.

(28) (a) Giacomelli, C.; Schmidt, V.; Borsali, R. *Macromolecules* **2007**, *40*, 2148−2157. (b) Zhang, X.; Rehm, S.; Safont-Sempere, M. M.; Würthner, F. *Nat. Chem.* **2009**, *1*, 623−629.

(29) (a) Panyam, J.; Labhasetwar, V. *Adv. Drug Delivery Rev.* **2003**, *55*, 329−347. (b) Nagae, M.; Hiraga, T.; Yoneda, T. *J. Bone Miner. Metab.* **2007**, *25*, 99−104.

(30) (a) Stubbs, M.; Mcsheehy, P. M. J.; Griffiths, J. R.; Bashford, C. L. *Mol. Med. Today* **2000**, *6*, 15−19. (b) Liu, G.; Li, X.; Xiong, S.; Li, L.; Chu, P. K.; Yeung, K. W. K.; Wu, S.; Xu, Z. *Colloid Polym. Sci.* **2012**, *290*, 349−357.